Physics-informed machine learning for understanding rock moisture dynamics in a sandstone cave

Kai-Gao Ouyang[1], Xiao-Wei Jiang[1,2*], Gang Mei[3], Hong-Bin Yan[4],

Ran Niu[1], Li Wan[1], Yijian Zeng[5]

1. MWR Key Laboratory of Groundwater Conservation, China University of Geosciences, Beijing, China

2. MNR Key Laboratory of Shallow Geothermal Energy, China University of Geosciences, Beijing, China

3. School of Engineering and Technology, China University of Geosciences, Beijing, China

4. Yungang Research Institute, Datong, Shanxi, China

5. Department of Water Resources, ITC Faculty of Geo-Information Science and Earth Observation, University of Twente, Enschede, the Netherlands

Correspondence: Xiao-Wei Jiang (jxw@cugb.edu.cn)

Abstract

Rock moisture, which is ~~considered as~~ a hidden component of the terrestrial hydrological cycle, has received little attention. In this study, the frequency-domain reflectometry ~~(FDR)~~ is used to monitor ~~obtain~~ fluctuating rock water content (RWC) in a sandstone cave of the Yungang Grottoes, China. We identified two major cycles of rock moisture addition and depletion, one in ~~the~~ summer ~~which is~~ affected by air vapor concentration, and the other in ~~the~~ winter caused by freezing-thawing. For the summer-time RWC, ~~By~~ by using the Long Short-Term Memory ~~LSTM~~ (LSTM~~Long Short-Term Memory~~) network and the SHapley Additive exPlanations ~~SHAP~~ (SHAP~~SHapley Additive exPlanations~~) method, we find relative humidity, air temperature and wall temperature ~~are found to~~ have contributions to rock moisture and there is a good match between predicted and measured RWC using the three variables as model inputs~~in the summer~~. Moreover, ~~B~~by using summer-time vapor concentration and the difference between dew point temperature and wall temperature as two input variables of the LSTM network, which belongs to physics-informed machine learning, the predicted RWC ~~rock water content~~ has a ~~very good~~better agreement with the measured ~~rock water content,~~RWC, ~~with the Nash–Sutcliffe efficiency~~

~~coefficient (NSE) being as high as 0.978. Because the two new input variables are factors directly controlling vapor condensation, they provide informative priors to the deep learning model and improved~~ ~~lead to better~~ ~~prediction performance,~~ with increased NSE and decreased MAE and RMSE. After identifying the causal factors of ~~rock water content~~RWC fluctuations, we also identified the mechanism controlling the ~~multi-diurnal~~ interday fluctuations of vapor condensation. The increased vapor concentration accompanying a precipitation event leads to transport of water vapor into rock pores, which is subsequently adsorbed onto the surface of rock pores and then condensed into liquid water. With the aid of the physics-informed deep learning model, this study increases understanding of sources of water in caves, which would contribute to future strategies of alleviating weathering in caves.

1 Introduction

Water movement in the unsaturated zone is a fundamental component of the hydrologic cycle regulating the atmosphere, the hydrosphere and the lithosphere (Arora et al., 2019; Brubaker and Entekhabi, 1996; Lu and Likos, 2004; Tindall et al., 1998). Although there are abundant studies on water movement in various scales of unsaturated soils (Larson et al., 2022; Schoups et al., 2005; Vereecken et al., 2014; Vinnikov et al., 1996; Yu et al., 2016), much less attention has been paid to water in unsaturated rocks. In a recent study, Rempe and Dietrich (2018) defined water stored in unsaturated rocks as rock moisture and pointed out that rock moisture is a hidden component of the terrestrial hydrologic cycle critical to ecosystems and weathering processes. Due to the ubiquitous occurrence of precipitation infiltration through unsaturated rocks, infiltrating precipitation was found to be the main source of rock moisture (Rempe et al., 2018; Sass, 2005). In fact, as early as in the fourth century BC, Aristotle (384-322 BC) hypothesized that atmospheric water vapor could penetrate into rocks in caves with low temperature and condense into liquid water (after Meinzer, 1934). Due to occurrence of hidden water in the form of rock moisture, many stone heritages inside caves have suffered from weathering (Auler and Smart, 2004; Camuffo, 1998; de Freitas et al., 2006; Guerriera et al., 2019; Linan et al., 2021). However, up to now, there is no observations of rock moisture in caves, which hampers a comprehensive understanding of the source and control factors of rock moisture.

By using such techniques as downhole neutron probe (Rempe and Dietrich, 2018), time domain reflectometry (TDR) (Salve et al., 2012) and nuclear magnetic resonance (NMR) (Schmidt and Rempe, 2020), the responses of rock moisture to precipitation were identified in some ~~small catchments~~previous studie.

However, these devices, ~~which~~ are usually long in length (~~the lengths of neutron probesare larger than 30 mm~~) or large in diameter (~~the diameter of NMR is around 70 mm~~), thus are not suitable to be used in stone heritages. For example, the lengths of neutron probes are larger than 300 mm, and the diameter of NMR is around 70 mm. In the recent two decades, ~~The~~ the frequency domain reflectometry (FDR), ~~which has the advantage of small in volume (the length is less than 60 mm),~~ has been widely used to characterize the temporal variability of soil moisture (Irmak and Irmak, 2005~~; Li et al., 2020~~; Xie et al., 2021; Zhang et al., 2019). Because FDR sensors have the advantage of small in volume (the length is less than 60 mm), for minimizing disturbance to ~~walls~~rocks in heritage sites, we attempt to use the FDR sensor to monitor rock moisture in a cave with stone carvings.

~~Note that both TDR and FDR measure the dielectric constant of porous media, and FDR is less influenced by temperature (Zhu et al., 2019). In this study, we attempt to use the FDR for monitoring rock moisture in the field for the first time and identify the atmospheric conditions controlling rock moisture in caves not exposed to rain.~~

Establishing the cause-and-effect relationship between rock moisture and various atmospheric conditions is a feasible approach to identify the source of rock moisture responsible for weathering in caves and to reveal mechanisms controlling cycles of rock moisture addition and depletion~~fluctuations~~. Machine learning has the ability to acquire knowledge and establish the complicated nonlinear relationship between variables in a vast domain (Chen et al., 2019a; Jumin et al., 2020). Although machine learning models have the ability of high accuracy prediction, they are notorious for being a black-box model. Lundberg and Lee (2017) proposed the SHAP (SHapley Additive exPlanations) values as a unified measure of feature importance, which led to a combination of accuracy and interpretability of predictions by machine learning models. In almost all applications of machine learning in the field of hydrology, the directly measured meteorological factors like precipitation, temperature, radiation, humidity and wind speed are used as input variables (e.g., Barzegar et al., 2017; Fang et al., 2017; Gao et al., 2020; Lees et al., 2021; Liu et al., 2022; Xiang et al., 2019; Zhao et al., 2022). In fact, the performance of a machine learning algorithm could be improved by using prior knowledge stemming from physical or mathematical understanding as model inputs ~~could improve the performance of a machine learning algorithm~~, which is called physics-informed learning (Karniadakis et al., 2021).

In this study, the ~~classic~~ Long Short-Term Memory (LSTM) network, which is a classic deep learning model, is combined with the SHAP values to predict rock moisture and evaluate the relative importance of four directly measured variables (precipitation, relative humidity, air temperature and wall temperature). After excluding the possible control by precipitation infiltration, based on the physics controlling vapor condensation,
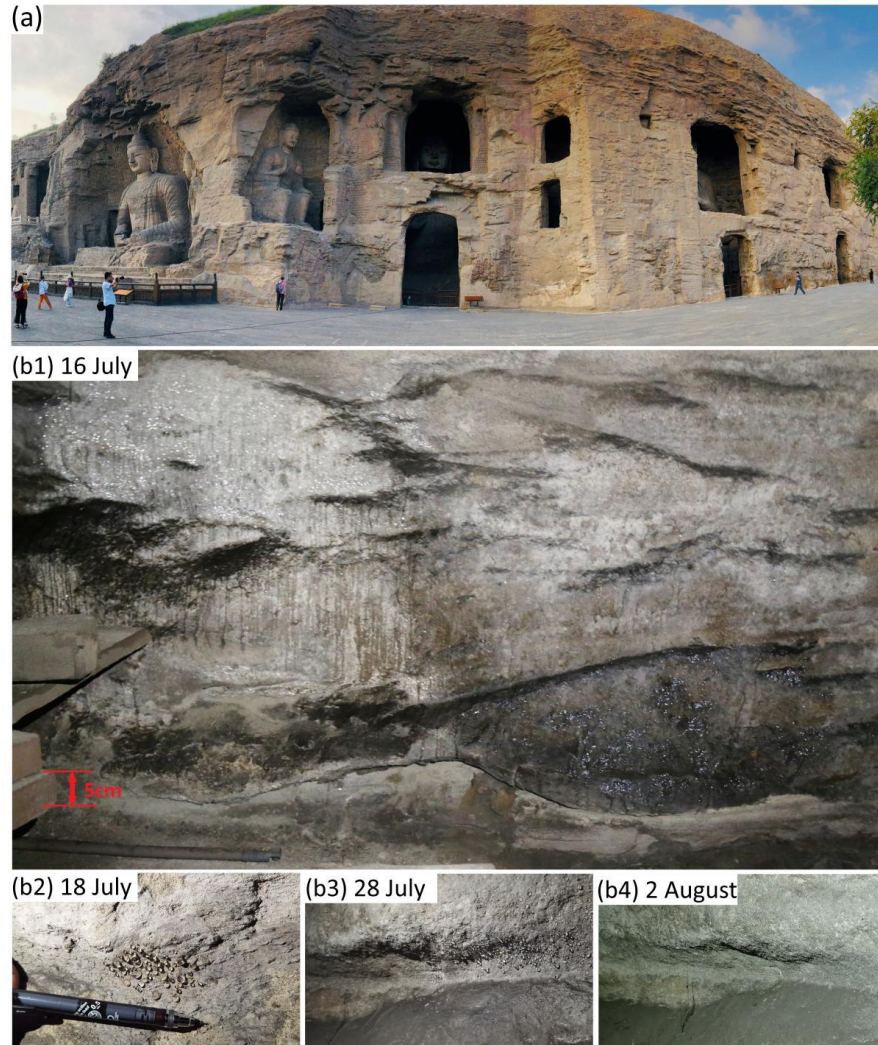
3

two new variables derived from relative humidity, air temperature and wall temperature are used as inputs of the LSTM network, which not only ~~leads to improved~~ improves prediction performance, but also leads to improved understanding of source of water in caves.

2 Study site and field monitoring

2.1. Study site

The Yungang Grottoes (40°07' N, 113°08' E), which are located in Datong, Shanxi Province, China, were declared World Heritage Site by the UNESCO in 2001 (http://whc.unesco.org/en/list/1039). According to meteorological data in recent 20 years (from 2002 to 2021) in the Datong city (data from ~~The~~ China Meteorological Data Service Center, http: //data.cma.cn/en), the ~~site~~ study area has a semi-arid climate, with an annual average precipitation of 393 mm and an annual average pan evaporation of 1243 mm. The precipitation in the rainy season from June to September accounts for 73% of the annual precipitation. The annual average temperature is 8 ℃, the average temperature in summer is 20.3 ℃, and the average temperature in winter is -8.2 ℃.

Most statues in the Yungang Grottoes were carved in sandstone caves in ~1500 years ago (Fig. 1a). In ~~the~~ summer, water droplets with planar distribution can be occasionally observed on the walls of some caves (Fig. 1b). Although no water droplets occur in other sandstone walls, by absorbing water, the high rock moisture leads to slight changes in the color of some walls. Water in the form of either water droplets or rock moisture ~~These different forms of water are~~ is responsible for weathering of the statues, however, the sources of ~~these~~ the two forms of water remain~~s~~ controversial. Previous studies suggested that the possible sources of water in caves include infiltrating precipitation through the overlying thick unsaturated zone (Wang et al., 2012) and condensation of water vapor onto walls (Cao et al., 2005; Huang, 2008; Huang, 2010).

Figure 1. (a) Some caves and statues in the Yungang Grottoes; (b) The occurrence (b1-b3) and disappearance (b4) of water droplets in Cave #5 of the Yungang Grottoes in the summer of 2021.

2.2. Monitoring of rock moisture and atmospheric conditions

To monitor variations of rock moisture in the shallow part of a cave wall, a FDR-based ~~ECH2O EC-5~~ sensor (ECH2O EC-5, produced by DECAGON, USA) was installed at 3-8 cm inside the north wall of Cave #9 (Fig. 2). Air temperature (T_a) and air relative humidity (RH) are simultaneously monitored near the monitoring site of rock moisture (Fig. 2). The wall temperature is also monitored to analyze whether the wall meets the condition for condensation. Moreover, hourly precipitation is available from a meteorological station outside the cave.

To make sure that the sensor is in close proximity to the porous rock, which is crucial to obtain accurate measurement, we use fine sand as infilling in the hole for the FDR sensor. ~~Due to the difficulty of calibrating the~~

5

~~actual water content in the field, the apparent rock water content measured by the sensor is directly used in the current study.~~ Because the FDR sensor is installed inside the cave without direct exposure to sunshine, there is limited diurnal fluctuations in wall temperature. Therefore, the influence of fluctuating temperature on rock water content (RWC) can be neglected, which is to be explained in detail in Section 4.1. As reported in previous experimental studies (Mollo and Greco, 2011; Sakaki and Rajaram, 2005), there is a good linear relationship between actual ~~rock water content~~RWC and rock moisture transformed from dielectric constant. Considering the difficulty of calibrating the actual water content in the field (Li et al., 2020; Sass,2005), and the purpose of the current study is to ~~identify~~ establish the ~~source~~ relationship between ~~of~~ rock moisture ~~addition~~ fluctuations and atmospheric conditions, ~~by establishing the relationship between rock moisture and atmospheric conditions, the relative changes of rock water content is more important than the actual value of rock water content. Therefore, direct use of apparent rock water content does not influence the results of our study, and~~ the apparent ~~rock water content~~RWC is directly ~~called~~ used as ~~rock water content~~RWC.
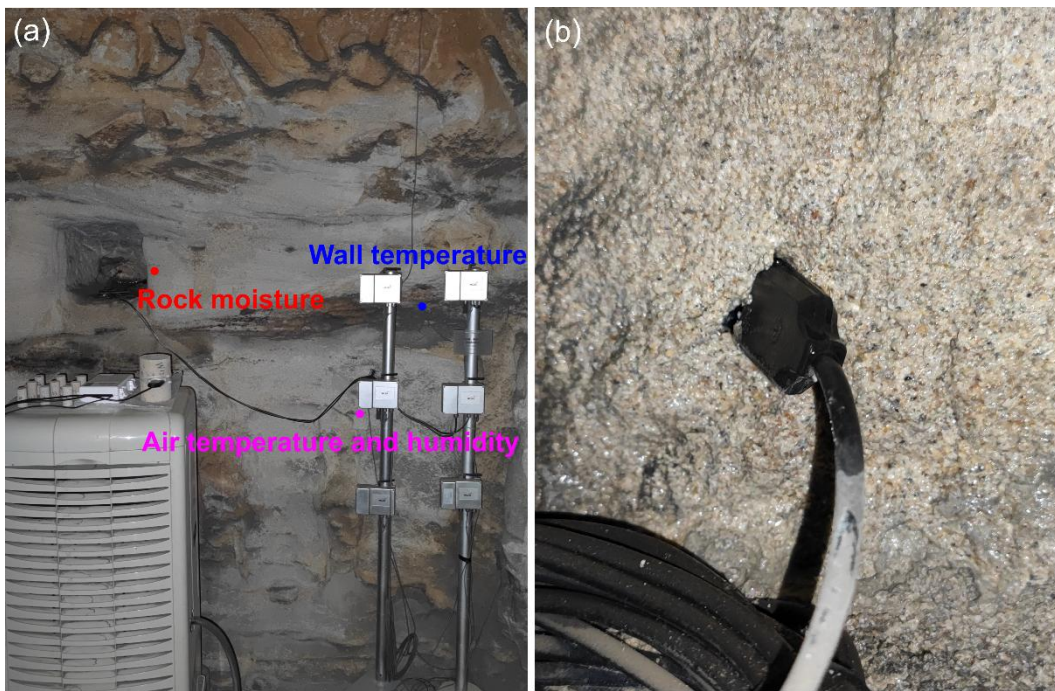

Figure 2. (a) The arrangements of sensors for rock moisture, wall temperature, air temperature and relative humidity in the north wall of Cave #9. (b) A photo showing ~~T~~the installed FDR sensor in Cave #9.

3 Methods

3.1 The ~~Long short-term memory (~~LSTM~~)~~ network

The LSTM network is an improved variant of the conventional Recurrent Neural Network (RNN), which is

140   a recurrent neural network that is mainly used for modeling sequence data. Because the LSTM network ~~and~~ has

the same fundamental framework as the conventional RNN, we first briefly introduce the structure of RNN. ~~RNN~~

~~is a recurrent neural network that is mainly used for modeling sequence data.~~ ~~Therefore, we first give a brief~~

~~introduction to the conventional RNN.~~ As shown in Fig. 3, ~~in the~~ a common RNN model consist of~~, there is~~ an

input layer, a hidden layer and an output layer~~.~~, where the hidden layer is used to capture features of sequence

145   data by RNN cells. x_t is the input vector at time step t, h_t is the hidden state at time step t determined by both the

input vector x_t at time step t and the hidden state (h_{t-1}) at time step t-1 (Zhao et al., 2017), and op_t is the output of

the RNN at time step t. Mathematically, the relationship between the three layers can be written as:

$$h_t = tanh\left(Ux_t + Wh_{t-1} + b_h\right)$$
      (1)

$$op_t = Vh_t + b_o$$
      (2)

150   where *tanh* is the activation function which means the hyperbolic tangent performs nonlinear transformations of

the inputs, *U*, *W* and *V* are the network weight matrices for input-to-hidden, hidden-to-hidden and

hidden-to-output connections, respectively, b_o and b_h are bias vectors.
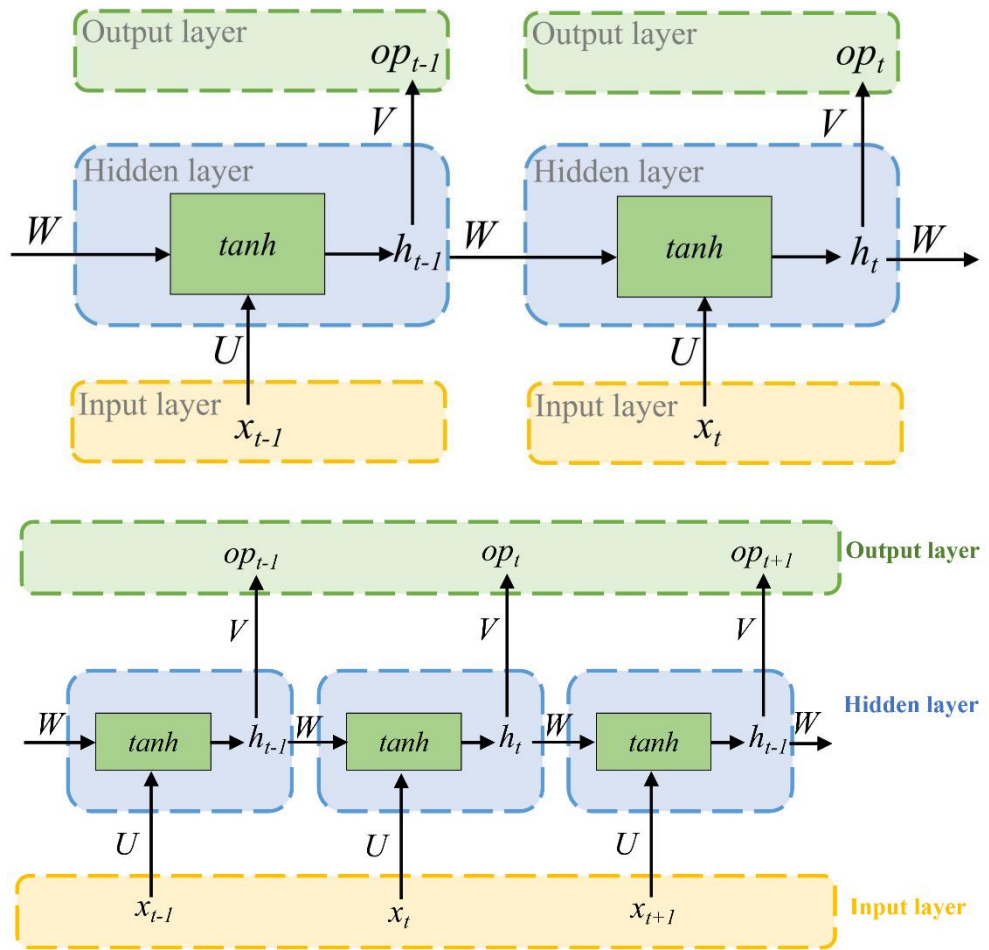
155   Figure 3. The structure of the Recurrent Neural Network (RNN) (Modified from Hopfield, 1982).

          The limitation of common RNNs is that they cannot capture the long time dependence of sequences, that is,

some earlier historical data are ignored when conducting predictions on long time series data~~When the time~~

~~sequence is too long, the RNN is not sufficiently efficient to learn because of vanishing gradient and exploding~~

160   ~~gradient problems~~ (Bengio, 1994; Hochreiter and Schmidhuber, 1997). To solve such problems, Hochreiter and

Schmidhuber (1997) proposed an improved variant of RNN whose hidden layer can capture the correlation

within time series in both short- and long--term dependence. ~~This improved variant,~~ which was named the LSTM

network~~,~~. In other words, the LSTM is a variant model that improve the limitation of common RNNs for

long-term dependence. ~~and its hidden layer was called the LSTM cell.~~ As shown in Fig. 4, ~~a~~ the LSTM replaces

165   the RNN cell in hidden layer with the LSTM cell, which introduces three types of ~~has three~~ gates:~~, including a~~

forget gate (f_t), ~~an~~ input gate (i_t) and ~~an~~ output gate (o_t). ~~, to maintain and adjust its cell state c_t (also called~~

~~memory) and hidden state h_t.~~ The forget gate determines the effect of the cell state c_{t-1} at the previous moment on

the current cell state c_t; the input gate determines the effect of the input x_t at the current moment on the cell state

c_t; and finally the output gate determines the effect of the cell state c_t on the output h_t ~~what information should be~~

170   ~~discarded from the cell state, the input gate specifies what new information need be stored in the cell state, and~~

~~the output gate determines what information from the cell state c_t should be passed to the next step~~ (Gao et al.,

2020; Fischer and Krauss, 2018; Lipton et al., 2015). ~~Note that in the input gate, the cell state is determined~~

~~simultaneously by the the sigmoid activation function which determines the weights of the information and the~~

~~tanh activation function which eliminates the bias of the network, the latter of which is termed abstract cell state.~~
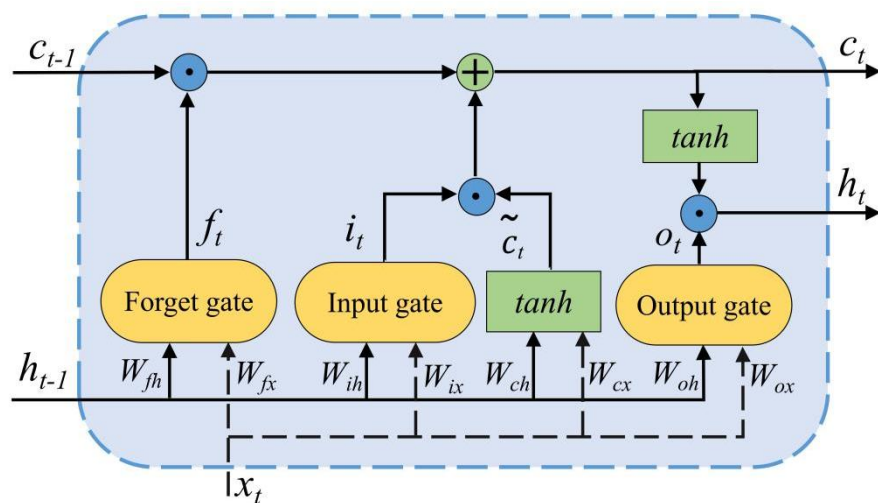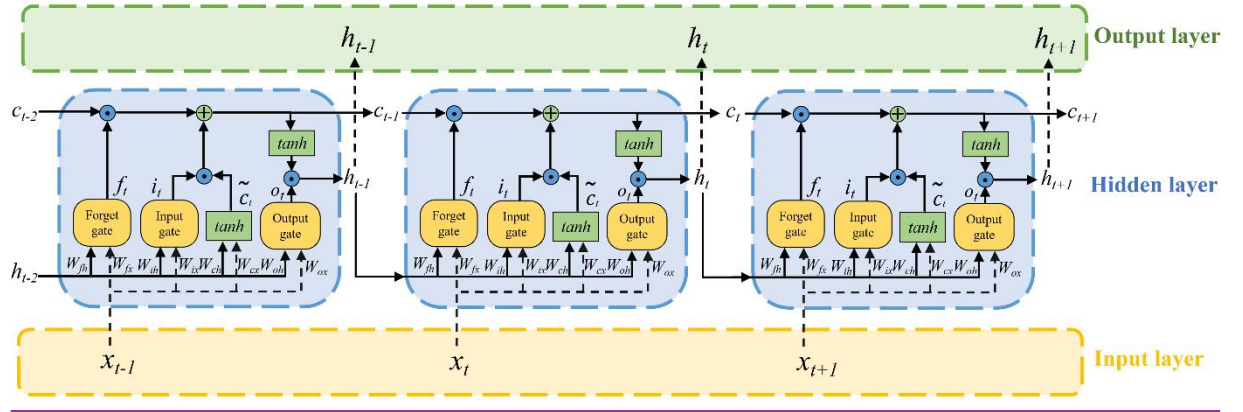

175

Figure 4. The structure of the LSTM cell (Modified from Hochreiter and Schmidhuber, 1997).

The formulas of the three gates, abstract cell state, cell state and hidden state in the LSTM cell are shown as follows:

$$\text{(forget gate)} \qquad f_t = \sigma\left(W_{fx}x_t + W_{fh}h_{t-1} + b_f\right) \tag{3}$$

$$\text{(input gate)} \qquad i_t = \sigma\left(W_{ix}x_t + W_{ih}h_{t-1} + b_i\right) \tag{4}$$

$$\text{(output gate)} \qquad o_t = \sigma\left(W_{ox}x_t + W_{oh}h_{t-1} + b_o\right) \tag{5}$$

$$\text{(abstract cell state)} \qquad \tilde{c}_t = tanh\left(W_{cx}x_t + W_{ch}h_{t-1} + b_c\right) \tag{6}$$

$$\text{(cell state)} \qquad c_t = f_t \odot c_{t-1} + i_t \odot \tilde{c}_t \tag{7}$$

$$\text{(hidden state)} \qquad h_t = o_t tanh \odot c_t \tag{8}$$

where i_t, f_t and o_t are the vectors of input, forget and output gates at time step t, respectively, all of which have the same sizes as c_t and h_t, σ is the logistic sigmoidal activation function, $\tilde{c}_t$ is the vector of abstract cell state at time step t, $\odot$ is element wise multiplication of two vectors. Similar to RNN, W_{fx}, W_{fh}, W_{ix}, W_{ih}, W_{ox}, W_{oh}, W_{cx} and W_{ch} are the matrices for different connections in the network, b_i, b_o and b_c are bias vectors. The dimensions of W_{fx}, W_{ix}, W_{ox} and W_{cx} are $D \times M$, and the dimensions of W_{fh}, W_{ih}, W_{oh} and W_{ch} are $M \times M$, where D is the number of input features and M is the number of hidden units in the LSTM layer. When M is large enough, an increasing M would lead to more computation time, but does not improve the prediction performance (Bengio, 2012).

In this study, the open-source framework TensorFlow (version 1.14.0) written in Python 3.7.6 is used to build and train the LSTM model. ~~The LSTM model effectively improves the gradient disappearance of RNNs in long time-series prediction by using gate structures, providing higher accuracy, which has been widely used in~~

~~many fields. In order to capture the more accurate temporal correlations between series data of rock water content (RWC).Although purely data-driven models may have a high accuracy of prediction, most machine learning models cannot extract interpretable information and knowledge from this data deluge (Karniadakis et al., 2021). The performance of machine learning models could be improved through providing physical prior knowledge. In this study,~~ We first use the raw atmospheric data (air relative humidity (RH), air temperature (T_a), precipitation (P) and wall temperature (T_w)) to predict RWC, then integrate physics controlling vapor condensation into the input variables to improve the performance of the LSTM model. In both schemes, we find the accuracy has stabilized when M equals 48.

3.2 Model interpretation and evaluation

To interpret the performance of a machine model, Lundberg and Lee (2017) proposed the SHAP (SHapley Additive exPlanations) explanation method, which is based on the game theory (Štrumbelj and Kononenko, 2014). The Shapely value of every input variable represents ~~the~~ its contribution ~~of it~~ on the prediction, and the importance of each input variable is clarified by comparing model performances with and without it. The formula for calculation of the Shapely value is

$$\varnothing_i = \sum_{S \subseteq F\{i\}} \frac{|S|!\left(F - |S| - 1\right)!}{n!} v\left(S \cup \{i\}\right) - v(S)$$

(9)

where ϕ_i is the contribution of variable i; F is the set of all input variables; $v(S \cup \{i\})$ is the result of a model trained with the variable i, and $v(S)$ is the result without the variable i, so the difference between them represents the effect of feature i on the model prediction. This method requires retraining the model on all feature subsets $S \subseteq F$ (Shapley, 1953).

To assess the accuracy of prediction by the LSTM network, we use the statistical metrics of Nash–Sutcliffe efficiency coefficient (NSE), mean absolute error (MAE) and root mean squared error (RMSE), all of which are widely used in the literature. NSE is the ratio of the sum of the squares of the regression to the total sum of the squares, which reflects the linear fit between the predictions and observations. The closer the value is to 1, the better the linear fit. The expression of NSE is

$$NSE = 1 - \frac{\sum_{i=1}^{N}\left(y_{Pred} - y\right)^2}{\sum_{i=1}^{N}\left(\overline{y} - y\right)^2}$$

(10)

where N is the number of data, and y_{Pred}, y, and $\overline{y}$ are the predicted, observed, and mean observed value, respectively. MAE is the mean of the distance between the predicted and the observations, whereas RMSE is the

square root of the mean of the square of the deviation between the predicted and the observations. The expressions of MAE and RMSE are

$$MAE = \frac{1}{N}\sum_{i=1}^{N}|y_{Pred} - y| \tag{11}$$

$$RMSE = \sqrt{\frac{1}{N}\sum_{i=1}^{N}(y_{Pred} - y)^2} \tag{12}$$

$$MAE = \frac{1}{N}\sum_{i=1}^{N}|y_{Pred}| - |y| \tag{11}$$

$$RMSE = \sqrt{\frac{1}{N}\sum_{i=1}^{N}(|y_{Pred}| - |y|)^2} \tag{12}$$

4 Results and discussion

4.1 The seasonal variations of rock moisture and atmospheric conditions

In the north wall of Cave #9, although there is no obvious occurrence of liquid water throughout the year, there is a clear trend of seasonal variations in ~~rock water content~~RWC (Fig. 5). Take the year 2021 for example, ~~F~~from ~~April~~ February to May, the ~~rock water content~~ RWC is relatively stable, ~~and maintains~~ maintaining at around 0.013 cm³/ cm³~~.~~; ~~f~~From June to September, which correspond to the rainy season with high relative humidity and high air temperature, there is a cycle of significant addition and depletion of rock moisture~~;~~. ~~f~~From October to December, there is a trend of gradual decrease in ~~rock water content~~RWC. The cycles of precipitation, relative humidity, air temperature and wall temperature from spring to early winter have quite similar trends as the cycle of ~~rock water content~~RWC, indicating that they are possible environmental conditions leading to the fluctuating ~~rock water content~~RWC.
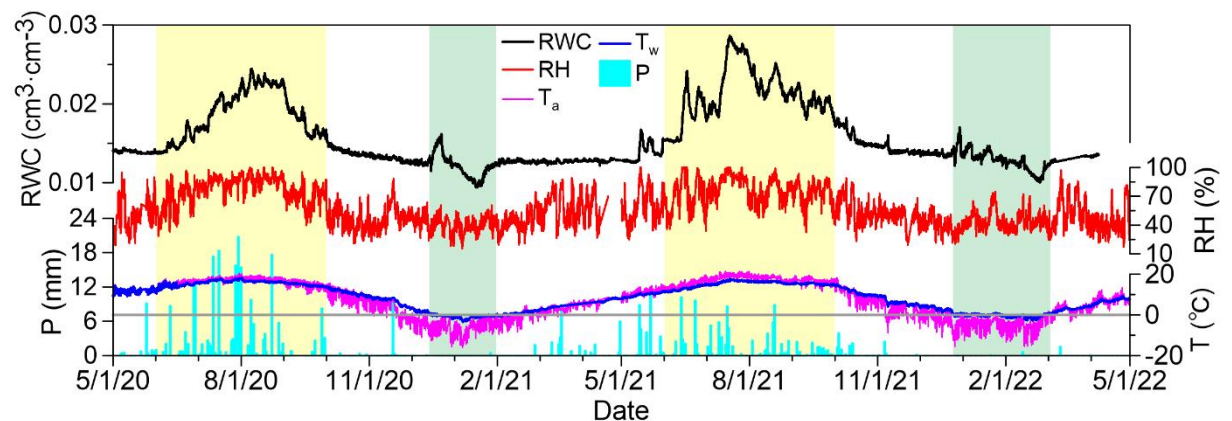
Figure 5. The temporal variations of rock water content (θRWC), air relative humidity (RH), air temperature (T_a),

precipitation (P) and wall temperature (T_w). The two periods in yellow correspond to the summer period with

245   high temperature and high humidity, whereas the two periods in green correspond to the fluctuation of rock

moisture caused by freezing-thawing.

    In the summer of 2021, the ~~rock water content~~RWC has a sharp increase since 9 July~~,~~ and is maintained at

relatively high values until 28 July, ~~reaches~~ with a maximum value equaling 0.029 cm³/ cm³ on 17 July. The high

250   ~~rock water content~~RWC indicates that there are atmospheric conditions responsible for water infiltration or water

vapor condensation ~~of water vapor~~. Note that this period with high RWC corresponds to the period with

occurrence of water droplets in Cave #5 as shown in Fig. 1b1-b3. Although there is no water droplet in Cave #9,

the color of the sandstone changes slightly, indicating that ~~a~~ this slight change ~~in the color of sandstone~~ is a result

of the ~~fluctuating~~ increas~~ing~~ed ~~rock water content~~RWC. Note that during the period from 11 July to 8 August

255   with RWC exceeding 0.021 cm³/ cm³, the daily wall temperature is quite stable, with an ~~daily~~intraday fluctuation

of around 0.8 °C ~~0.0007 cm³/ cm³~~(Fig. 6a). The obvious trend of increasing and decreasing RWC accompanying

the relatively stable wall temperature indicates that the effect of increasing RWC caused by rising temperature

can be excluded. Therefore, we believe that the ~~rock water content measured by~~ FDR readings reflect~~s~~ the actual

change of ~~water content in the rock~~RWC.
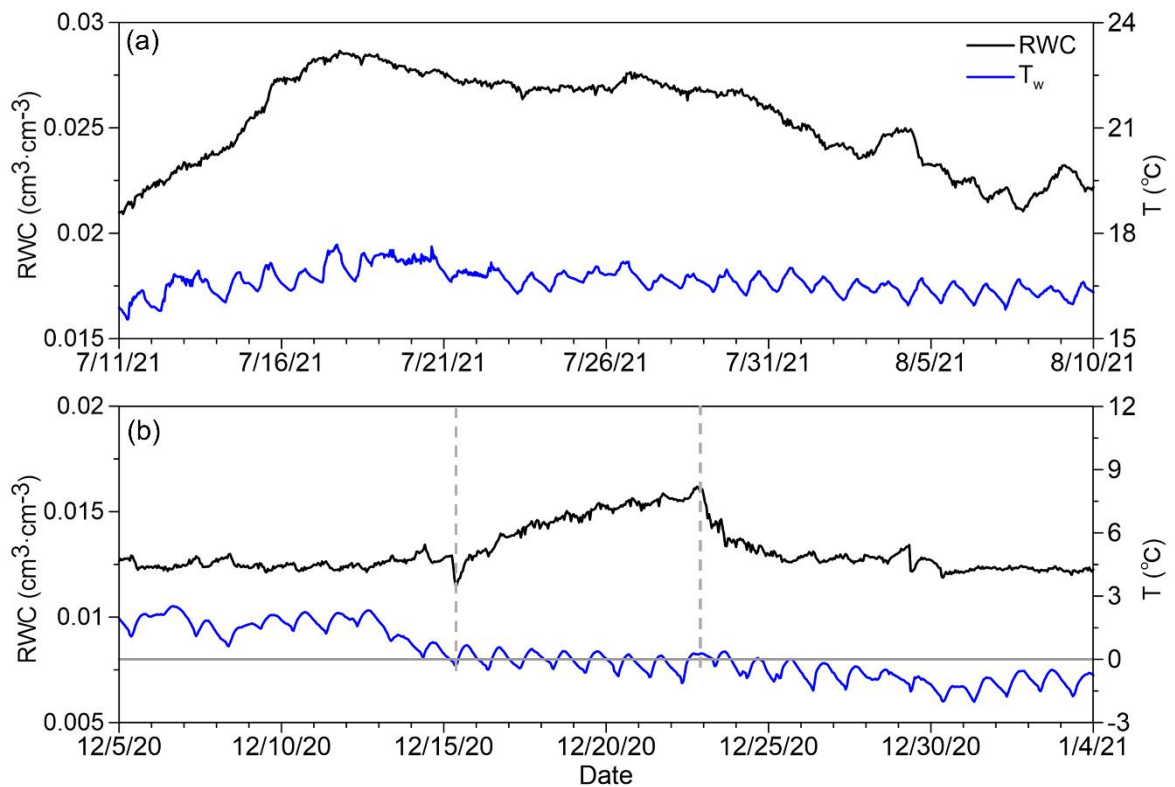
260

Figure 6. Two typical periods with obvious rock moisture addition but no trends of increasing temperature. (a) From 11 July 2021 to 10 August 2021; (b) From 15 December 2020 to 23 December 2020.

From mid December 2020 to the end of January 2021, and from late December 2021 to the end of February 2022, there are also significant fluctuations of RWC (Fig. 5). This pattern of fluctuation is a direct consequence of freezing-thawing, which can be confirmed by the negative wall temperature. At the beginning of the freezing-thawing cycle, there is a trend of increasing RWC due to freezing-induced liquid water migration towards the wall surface with the lowest temperature. Because the trend of increasing RWC accompanies a relatively stable wall temperature with a mean of around 0 ℃ (Fig. 6b), we believe that the FDR readings in winter also reflect the actual change of RWC. By the end of the freezing period, the RWC reaches a minimum value of the year because most liquid water has been transformed into ice. In the two years, the minimum liquid water content is 0.009 cm^3/ cm^3 (on 16 January 2021) and 0.010 cm^3/ cm^3 (on 25 February 2022), respectively. In the thawing stage, there is a trend of increasing liquid water content.

The pattern of freezing-thawing-induced RWC fluctuations is similar to that of freezing-thawing-induced soil water content fluctuations (Deprez et al., 2020; Matsuoka and Murton, 2008; Sun and Scherer, 2010; Xie et al., 2021; Yu et al., 2018), demonstrating that the FDR technique is very sensitive to liquid water content in sandstone and is suitable to measure rock moisture. The fluctuating RWC during the freezing-thawing cycle also has implications for understanding weathering processes. The increased RWC before freezing indicates that there is movable water in winter even if the RWC is very low. The decreasing low liquid water content induced by freezing indicates that rock moisture in spring and autumn belongs to movable bound water that could be responsible for chemical weathering. The movable water could be responsible for chemical weathering , and the freezing of liquid water near the wall surface might cause physical weathering. Therefore, our field monitoring of RWC in winter has implications for understanding rock weathering.

4.2 The performance of the LSTM model with two different schemes of model inputs

In the rainy season, as we pointed out in 4.1, precipitation, relative humidity, air temperature and wall temperature have quite similar trends of seasonal variations as RWC. Apparently, they are all possible factors determining the fluctuating apparent rock moisture. Therefore, in 4.2.1, we first use all of

290 them as input variables (scheme #1) of the LSTM model to predict ~~rock water content~~RWC, and use the SHAP values to evaluate the contribution of each input variable. After excluding precipitation whose mean |SHAP value| equals 0, in 4.2.2, we use two new parameters (vapor concentration, dew point temperature minus wall temperature) calculated from relative humidity, air temperature and wall temperature as input variables (scheme #2) of the LSTM model to predict ~~apparent rock moisture~~RWC.

295 Deep learning models require a large amount of data for training, as well as data sets with a longtime span to ensure the mastery of complete data features. Because the period from 1 June to 1 October has the most significant trends of rock moisture addition and depletion, the hourly data during this period in the year 2020 are used to construct the training set, whereas the hourly data in the year 2021 are used to construct the test set.

4.2.1 The predicted results based on directly monitored variables

300 By using relative humidity, air temperature, precipitation and wall temperature as model input variables, there is a fairly good match between the predicted and measured ~~rock water content~~RWC, with similar patterns of fluctuations (Fig. 76a). Although there is obvious underestimation of ~~rock water content~~RWC in mid and late July, and slight underestimation or overestimation in other months, the NSE is as high as 0.958, indicating that the fluctuating relative humidity, air temperature, precipitation and wall temperature can capture the major patterns of 305 the fluctuating ~~rock water content~~RWC.
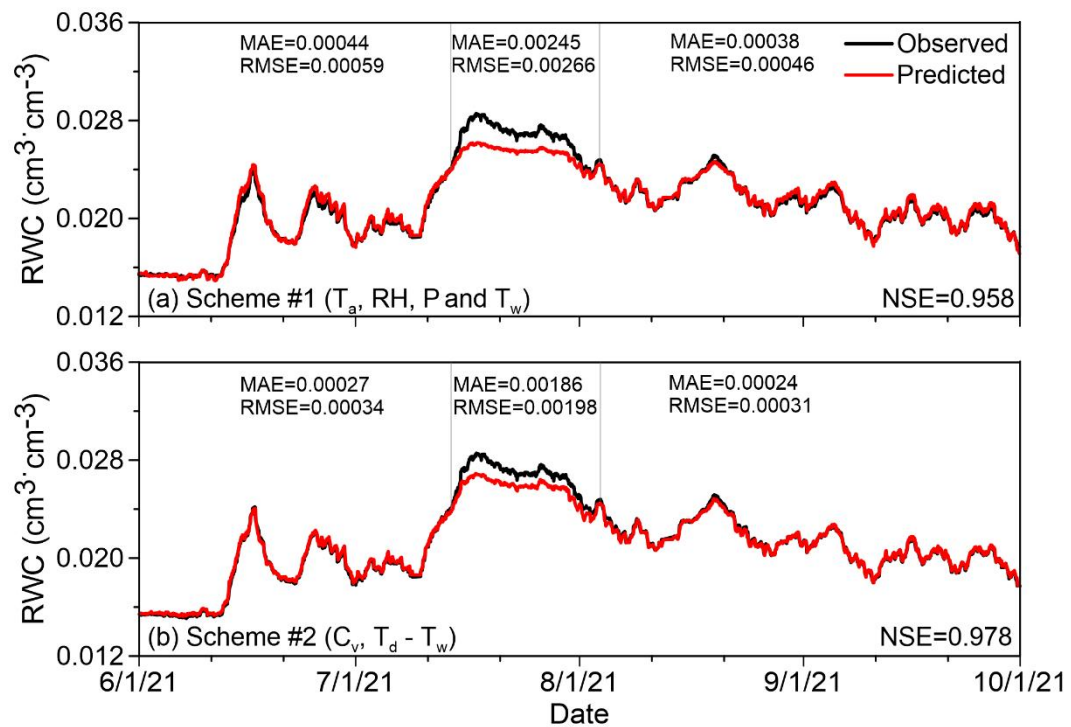

Figure 76. The predicted and measured ~~rock water content~~RWC obtained by two schemes. (a) Scheme #1 using

four directly measured variables; (b) Scheme #2 using two calculated variables controlling vapor condensation. Also shown are NSE of the whole time series, MAE and RMSE of three different stages.

310

Fig. 8~~7~~a shows the mean absolute SHAP value of each input variable, which represents the relative importance of each variable for the prediction. The mean absolute SHAP values are in descending order: ~~of~~ air relative humidity (0.0087), air temperature (0.0032), wall temperature (0.0018), ~~rock water content~~RWC at previous time step (0.0004) and precipitation (0) ~~are 0.0087, 0.0032, 0.0018, 0.0004 and 0,~~ respectively.

315 Therefore, precipitation infiltration has no direct contribution to rock moisture in caves, and we infer that vapor condensation should be the source of rock moisture in caves.
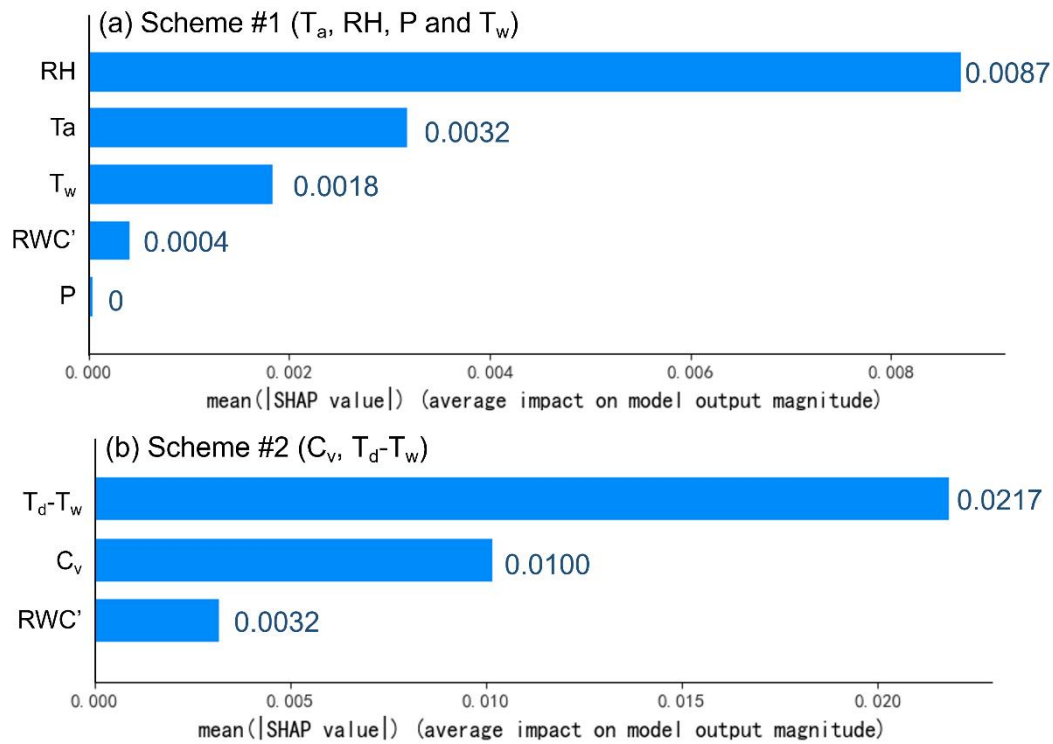

Figure 8~~7~~. The relative importance of each input variable in the two schemes with different input variables. (a) Scheme #1 using four directly measured variables; (b) Scheme #2 using two calculated variables controlling

320 vapor condensation. Note that ~~rock water content~~RWC at previous step ($\theta RWC'$) also has contribution to prediction.

4.2.2 The prediction results based on variables controlling vapor condensation

Based on the SHAP values of scheme #1, precipitation can be excluded as an input variable for the LSTM

325 network. Among the three directly monitored variables that have contributions to ~~rock water content~~RWC, air

15

relative humidity and air temperature determines the vapor concentration and the dew point temperature (Nguyen et al., 2014), and whether the wall temperature is below the dew point temperature determines whether vapor condensation could occur (Fernández-Cortés et al., 2006; Gabrovšek et al., 2010; Li et al., 2021). Because water vapor is the direct source of condensation water and whether the wall temperature is below the dew point temperature is the precondition of vapor condensation, we use vapor concentration and dew point temperature minus wall temperature as two input variables, both of which are direct variables controlling vapor condensation.

Vapor concentration and dew point temperature are both functions of actual vapor pressure, which is determined by air temperature, saturated vapor pressure and relative humidity. For air with a temperature of T (K), the formulas for calculating saturated vapor pressure and actual vapor pressure are (Lawrence, 2002; Lu, 2004):

$$u_{v,sat} = 0.611 \exp\left(17.27 \frac{T-273.2}{T-36}\right) \tag{13}$$

$$u_v = u_{v,sat} \cdot RH \tag{14}$$

where $u_{v,sat}$ is the saturation vapor pressure (kPa), RH is the relative humidity of air (%), and u_v is the actual vapor pressure (kPa). After obtaining u_v, we can calculate the vapor concentration, C_v (g/m^3), and the dew point temperature, T_d (K). The equations of C_v and T_d are, can be calculated as (Lu, 2004)

$$C_v = 217 \cdot \frac{u_v}{T-273.15} \tag{15}$$

$$T_d = \frac{36 \ln(u_v) - 4700}{\ln(u_v) - 16.78} \tag{16}$$

As indicated in Equation 156, a higher water vapor pressure content in the air, u_v, corresponds to a higher vapor concentrationdew point temperature, thus a higher possibility of condensation at the wall. Fig. 98 shows that the patterns of fluctuating rock water contentRWC, vapor concentration and difference between dew point temperature and wall temperature (denoted as T_d-T_w hereafter) in the whole non-freezing period are quite similar. Moreover, we find the period with a positive T_d-T_w has a good correspondence with the period with a high level of rock moisture.
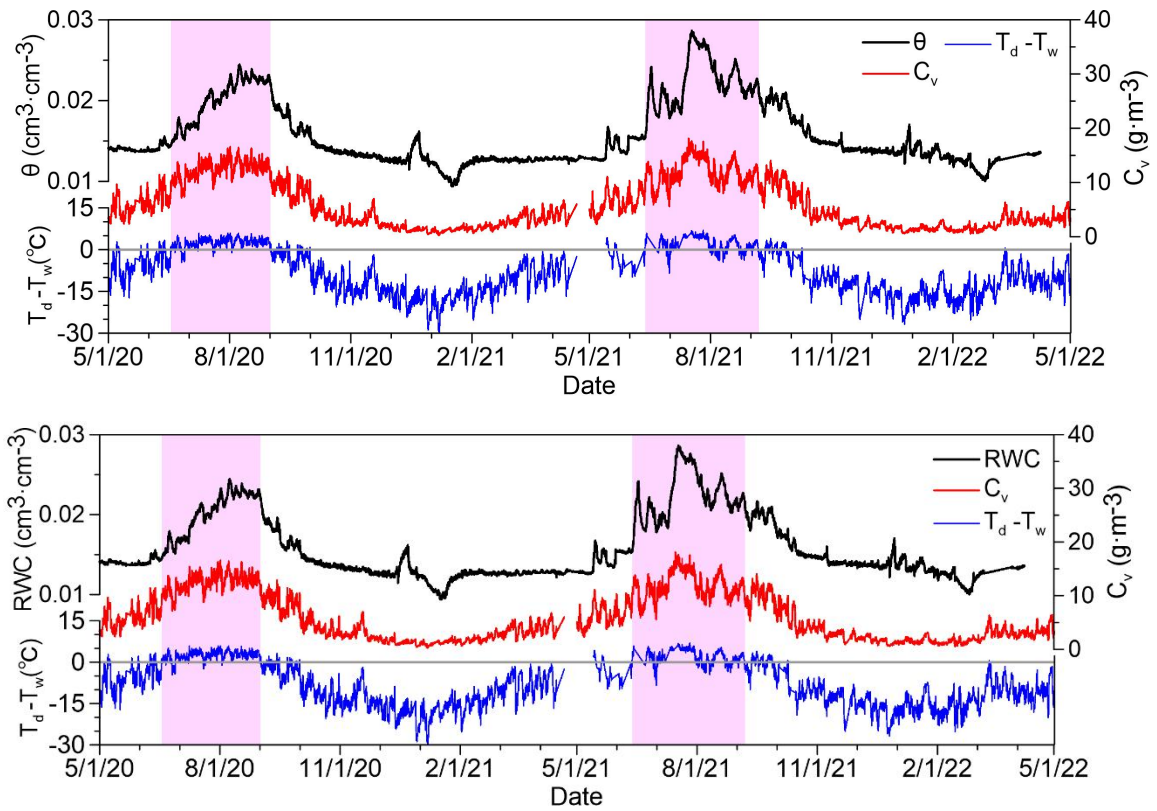
Figure 98. The fluctuating apparent rock moisture (*RWCθ*), vapor concentration (C_v), and the difference between dew point temperature and wall temperature (T_d-T_w). The zones in purple represents the periods with positive T_d-T_w and high rock moisture.

In scheme #2, by using the two new variables as inputs of the LSTM model, the mean absolute SHAP values of T_d-T_w and vapor concentration are 0.0217 and 0.0100, respectively (Fig. 87b), indicating that both variables have significant contributions to rock moisture. Moreover, the NSE of predicted rock moisture is ~~further~~ increased to 0.978 (Fig. 76b). Although the prediction still underestimates ~~rock water content~~RWC from mid July to the end of July, the MAE reduced from 0.245 in scheme #1 to 0.186 in scheme #2, and the RMSE reduced from 0.01416 in scheme #1 to 0.01050 in scheme #2. In the other two time durations shown in Fig. 7b, the MAE and the RMSE of scheme #2 also decrease obviously. Therefore, scheme #2 has much better performance of prediction, showing that using physics-informed variables would improve accuracy of prediction.

4.3 The mechanism of water vapor condensation

As we illustrated in 4.2, precipitation is not directly responsible for rock moisture fluctuations, but other atmospheric conditions controlling vapor concentration and the condition of vapor condensation are directly responsible for ~~rock moisture~~RWC fluctuations in the cave. In fact, vapor concentration fluctuations are more or less related to precipitation events. As shown in Fig. 109, the vapor concentration usually begins to rise ~~prior to~~

~~the occurrence of~~before a precipitation event, and declines under the control of solar radiation after a precipitation event.

Under the control of convection and diffusion, the increased water vapor in the air could be transported into porous media. When the sandstone is dry, water vapor can be adsorbed onto the surface of the rock pores, forming an adsorbed layer as thin water film; as curved menisci begin to form under increasing relative humidity, capillary condensation occurs in the rock pores (Broekhoff, 1969; Lu and Likos, 2004; Xu et al., 1998). Both adsorption and capillary condensation would lead to rock moisture addition. As shown in Fig. 10~~9~~, in ~~the~~ summer of 2021, there are 10 stages with obvious rock moisture additions. In the majority of the 10 stages, there are lagged responses of rock moisture additions to rising vapor concentration in the air, probably due to time required for vapor convection and diffusion.

Among the 10 stages, the magnitude of rock moisture addition is controlled by T_d-T_w. In stages IV, V, VII, VIII, IX and X, because the dew point temperature seldom exceeds the wall temperature, the magnitudes of rock moisture additions are relatively small. In stages I, II, III and VI, there are long durations with dew point temperature being higher than the wall temperature, causing large magnitudes of rock moisture addition. However, at the beginning of these four stages, even if dew point temperature is still lower than the wall temperature, increasing vapor concentration has resulted in rock moisture addition. Therefore, although a negative T_d-T_w does not exclude the possible occurrence of capillary condensation, a positive T_d-T_w does promote capillary condensation.

After ~~Following~~ the 10 stages of rock moisture additions, we find rock moisture depletions are ~~is~~ very sensitive to decreasing vapor concentration. Moreover, inside ~~in~~ stage III with very high ~~rock water content~~RWC, a slight decrease in vapor concentration results in a slight decrease in ~~rock water content~~RWC. Therefore, we believe that ~~rock water content~~RWC measured by the FDR technique is sensitive enough to fluctuating vapor concentrations and can be applied in future rock moisture monitoring in other settings.

370

375

380

385
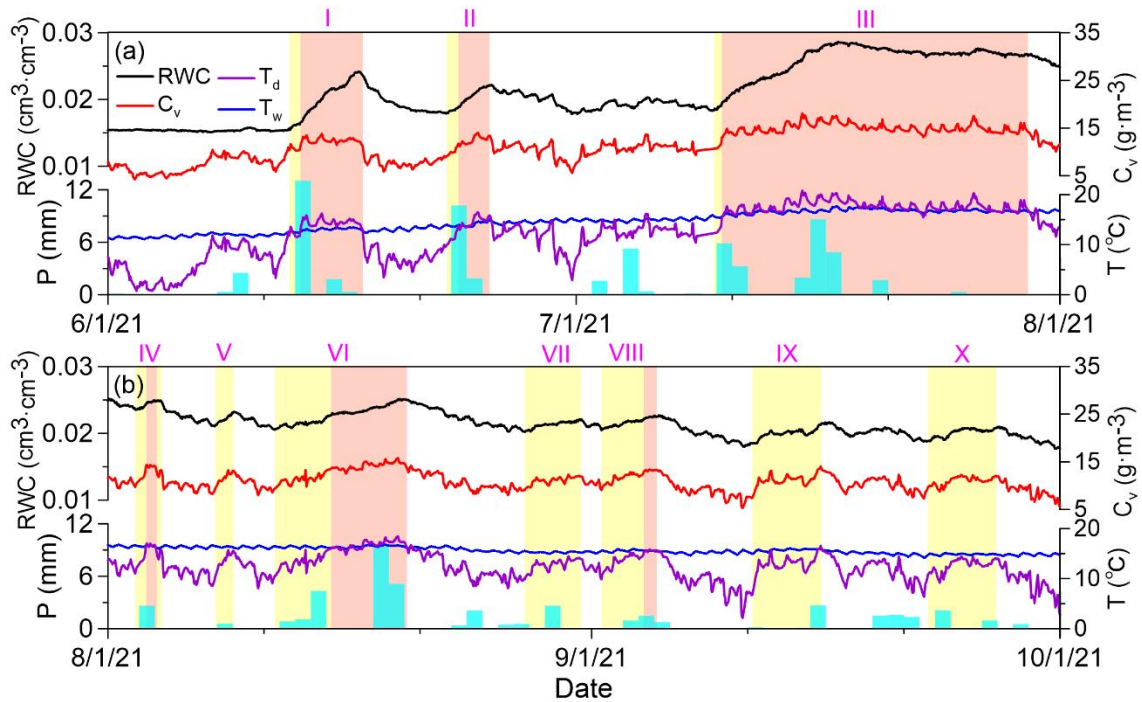
Figure. ~~1~~0~~9~~. Plots showing the responses of rock water content (θ RWC) to precipitation (P), vapor concentration (C_v), dew point temperature (T_d) and wall temperature (T_w) in the summer of 2021. The zones in yellow have increasing ~~rock water content~~ RWC, and zones in red have increasing ~~rock water content~~ RWC as well as positive T_d-T_w.

5 Conclusion

The source of water in the sandstones caves in the Yungang Grottoes responsible for weathering was a long-standing unresolved scientific question. In this study, we use the FDR sensor to monitor the rock moisture in a cave, which shows clear rock moisture addition-depletion~~s~~ cycles due to various controlling mechanisms. By using relative humidity, air temperature, precipitation and wall temperature as the input variables of the LSTM network, the predicted rock moisture well reproduced the pattern of monitored rock moisture fluctuations. Moreover, we find that precipitation has no contribution, but all other three variables have contribution to the fluctuating rock moisture. Because relative humidity, air temperature and wall temperature belong to factors controlling vapor condensation, this scheme of deep learning reveals that vapor condensation instead of precipitation infiltration is the source of rock moisture in the cave.

By calculating vapor concentration and dew point temperature from air temperature and relative humidity, we proposed two new variables, vapor concentration and the difference between dew point temperature and wall temperature as input variables of the LSTM network. Because the two variables are direct controlling factors of

19

vapor condensation, this scheme leads to a much better accuracy of prediction, confirming that rock moisture in the cave is derived from vapor condensation. We also analyzed how precipitation events control vapor concentration, thus indirectly control vapor condensation inside the rock.

By monitoring rock moisture in the field and examining their responses sensitiveness of rock moisture to atmospheric conditionsvapor concentration and the difference between dew point temperature and wall temperature, this study demonstrates for the first time that the FDR technique is an effective means for monitoring rock moisture. By using variables directly controlling vapor condensation as the input variables of the LSTM model, this study shows that "physics-informed" deep learning can improve prediction performance. Moreover, by identifying how vapor condensation controls rock moisture and occasional occurrence of water droplets in the study area, this study contributes to the understanding of the sources of water in caves, which is important in providing scientific-based proofs to propose future strategies for alleviating weathering of stone heritages.

Code availability.

All code used to generate, train, and test the models are available in a dedicated Zenodo repository: https://doi.org/10.5281/zenodo.7382827.

Data availability.

The data of rock water content and atmospheric conditions at the field site (from 1 May 2020 to 1 May 2022) are available in a dedicated Zenodo repository: https://doi.org/10.5281/zenodo.7382895.

Author contributions.

All authors were involved in interpretating data provided by HY. XJ developed the initial idea of the current study, and KO run the models with the help of GM. KO and XJ wrote the manuscript with contributions from GM and YZ.

Competing interests.

The authors declare that they have no conflict of interest.

Special issue statement.

This article is part of the special issue "Experiments in Hydrology and Hydraulics". It is not associated with a conference.

References

Arora, B., Dwivedi, D., Faybishenko, B., Jana, R. B. and Wainwright, H. M.: Understanding and predicting
445   vadose zone processes, Rev. Mineral Geochem., 85, 303–328, https://doi.org/10.2138/rmg.2019.85.10, 2019.

Auler, A. S. and Smart, P. L.: Rates of condensation corrosion in speleothems of semiarid northeastern Brazil, Speleogenesis Evol. Karst Aquifers, 2, 2004.

Barzegar, R., Fijani, E., Moghaddam, A, A. and Tziritis E.: Forecasting of groundwater level fluctuations using ensemble hybrid multi-wavelet neural network-based models, Sci. Total. Environ., 599–600, 20–31,
450   https://doi.org/10.1016/j.scitotenv.2017.04.189, 2017.

Bengio, Y., Simard, P. and Frasconi, P.: Learning long-term dependencies with gradient descent is difficult, IEEE Trans. Neural Netw. Learn Syst., 5, 157–166, https://doi.org/10.1109/72.279181, 1994.

Bengio, Y.: Practical recommendations for gradient-based training of deep architectures, in: Neural networks: Tricks of the trade, edited by: Montavon, G., Orr, G. B., and Müller, K.-R., Springer, 437–478,
455   https://doi.org/10.1007/978-3-642-35289-8_26, 2012.

Broekhoff, J., C., P.: Sorption and Capillarity, Waltman, Delft, 1969.

Brubaker, K. L. and Entekhabi, D.:Analysis of feedback mechanisms in land-atmosphere interaction, Water Resour. Res., 32, 1343–1357, https://doi.org/10.1029/96WR00005, 1996.

Camuffo, D.: Microclimate for cultural heritage. Elsevier, Amsterdam, 1998.

460   Cao, W. B., Wan, L., Zeng, Y. J., Gan, X. M., Jiang, X. W., Huang, J. Z., Yan, H. B. and Zhang, L. Study on formation mechanism and prevention of condensation water in Yungang Grottoes, in: Collection of Papers of the 2005 Yungang International Academic Seminar (Protection Volume). Cultural Relics Publishing House, Beijing, 191–198, 2005. (in Chinese)

Chen, J., Gao, X., Zheng, X., Miao, C., Zhang, Y., Du, Q., and Xu, Y.: Simulation of Soil Freezing and Thawing

465   for Different Groundwater Table Depths, Vadose Zone J., 18, 18057, https://doi.org/10.2136/vzj2018.08.0157, 2019.

De Freitas, C. R., Schmekal, A.: Studies of condensation/evaporation processes in the Glowworm Cave, New Zealand. Int. J. Speleol., 35, 75–81, http://dx.doi.org/10.5038/1827-806X.35.2.3, 2006.

Deprez M., De Kock, T., De Schutterc, G. and Cnudde, V.: A review on freeze–thaw action and weathering of

470   rocks, Earth–Sci. Rev. 203, 103143, 2020.

Fernández-Cortés, Á., Calaforra, J.M. and García-Guinea, J.: The Pulpí gigantic geode (Almería, Spain): geology, metal pollution, microclimatology, and conservation, Environ. Geol., 50, 707–716, https://doi.org/10.1007/s00254-006-0243-z, 2006.

Fang, K., Pan, M. and Shen, C. P.: The value of SMAP for long-term soil moisture estimation with the help of

475   deep learning, IEEE T. Geosci. Remote, 57, 2221–2233, https://doi.org/10.1109/TGRS.2018.2872131, 2019.

Fischer, T. and Krauss, C.: Deep learning with long short-term memory networks for financial market predictions, Eur. J. Oper. Res., 270, 654–669, https://doi.org/10.1016/j.ejor.2017.11.054, 2018.

Gabrovšek, F., Dreybrodt, W. and Perne, M., Physics of condensation corrosion in caves. In: Advances in Research in Karst Media. Environmental Earth Sciences, edited by: Andreo, B., Carrasco, F., Durán, J. J.

480   and LaMoreaux, J. W., Springer, Berlin, Heidelberg, 491–496, https://doi.org/10.1007/978-3-642-12486-0_75, 2010.

Gao, S., Huang Y. F. Zhang, S., Han, J. C., Wang, G. Q., Zhang, M. X. and Lin, Q. S.: Short-term runoff prediction with GRU and LSTM networks without requiring time step optimization during sample generation, J. Hydrol., 589, 125188, https://doi.org/10.1016/j.jhydrol.2020.125188, 2020.

485   Guerrier, B., Doumenc, F., Roux, A., Mergui, S. and Jeannin, P.Y.: Climatology in shallow caves with negligible ventilation: Heat and mass transfer. Int. J. Therm. Sci., 146, 106066, https://doi.org/10.1016/j.ijthermalsci.2019.106066, 2019.

Hochreiter, S. and Schmidhuber, J.: Long Short-Term Memory, Neural Comput., 9, 1735–1780, https://doi.org/10.1162/neco.1997.9.8.1735, 1997.

490   Hopfield, J. J.: Neural networks and physical systems with emergent collective computational abilities, P. Natl. Acad. Sci. USA, 79, 2554–2558, https://doi.org/10.1073/pnas.79.8.2554, 1982.

Huang, K. Z.: Harm and Prevention of Water in Yungang Grottoes, in: Cultural relics protection technology (1981-1991), China Science Publishing & Media Ltd, Beijing, 284–290, 2010. (in Chinese)

Huang, J. Z.: Waterproof protection of Yungang Grottoes, a world cultural heritage. Sciences of Conservation and

495   Archaeology, 20, 114–121, 2008. (in Chinese)

Huang, J. Z., Wan, L., Peng, T., Cao, W. B. and Wang, X. S.: Survey on water sources in Yungang Grottoes and some results. Geotechnical Investigation & Surveying, 40,1–5, 2012. (in Chinese)

Irmak, S. and Irmak, A.: Performance of frequency-domain reflectometer, capacitance, and psuedo-transit time-based soil water content probes in four coarse-textured soils, Appl. Eng. Agric., 21, 999 – 1008, https://doi.org/10.13031/2013.20035, 2005.

Jumin E.,Zaini, N.,Ahmed A. N.,Abdullah, S.,Ismail, M., Sherif, M.,Sefelnasr, A. and Ahmed El-Shafie, A.: Machine learning versus linear regression modelling approach for accurate ozone concentrations prediction, Eng. Appl. Comp. Fluid, 14, 713-725, https://doi.org/10.1080/19942060.2020.1758792, 2020.

Karniadakis, G. E., Kevrekidis, I. G., Lu, L., Perdikaris, P., Wang, S. F. and Yang, L.: Physics-informed machine learning. Nat. Rev. Phys., 3, 422–440, https://doi.org/10.1038/s42254-021-00314-5, 2021.

Larson, J., Lidberg, W., Ågren, A. M. and Laudon, H.: Predicting soil moisture conditions across a heterogeneous boreal catchment using terrain indices, Hydrol. Earth Syst. Sci., 26, 4837–4851, https://doi.org/10.5194/hess-26-4837-2022, 2022

Lawrence, D. S.: Physical hydrology, Prentice Hall, Upper Saddle River, 2002.

Lees, T., Buechel, M., Anderson, B., Slater, L., Reece, S., Coxon, G. and Dadson, S. J.:Benchmarking data-driven rainfall–runoff models in Great Britain: a comparison of long short-term memory (LSTM)-based models with four lumped conceptual models, Hydrol. Earth Syst. Sci., 25, 5517–5534, https://doi.org/10.5194/hess-25-5517-2021, 2021.

Li, P. J., Zha, Y. Y., Tso, C. M., Shi, L. S., Yu, D. Y., Zhang, Y. G. and Zeng, W. Z.: Data assimilation of uncalibrated soil moisture measurements from frequency-domain reflectometry, Geoderma, 374, 114432, https://doi.org/10.1016/j.geoderma.2020.114432, 2020.

Li, Y. F., Aemisegger. F., Riedl, A., Buchmann, N. and Eugster, W.: The role of dew and radiation fog inputs in the local water cycling of a temperate grassland during dry spells in central Europe, Hydrol. Earth Syst. Sci., 25, 2617–2648, https://doi.org/10.5194/hess-25-2617-2021, 2021.

Liñán, C., Benavente, J., del Rosal, Y., Vadillo, I., Ojeda, L. and Carrasco, F.: Condensation water in heritage touristic caves: Isotopic and hydrochemical data and a new approach for its quantification through image analysis, Hydrol. Process, 35, e14083. https://doi.org/10.1002/hyp.14083, 2021.

Lipton, Z. C.: Berkowitz, J. and Elkan, C.: A critical review of recurrent neural networks for sequence learning, arXiv [preprint], arXiv: 1506.00019, https://doi.org/10.48550/arXiv.1506.00019, 2015.

525   Liu, G. J., Tang, Z. Y., Qin, H., Liu, S., Shen, Q., Qu, Y. H., Zhou, J. Z.: Short-term runoff prediction using deep learning multi-dimensional ensemble method, 609, 127762, https://doi.org/10.1016/j.jhydrol.2022.127570, 2022.

Lundberg, S. M. and Lee, S.: A unified approach to interpreting model predictions, in: Advances in neural information processing systems 30 (NIPS 2017), edited by: Guyon, I., Luxburg, U. V., Bengio, S., Wallach,

530   H., Fergus, R., Vishwanathan, S. and Garnett, R., Neural information processing systems (NIPS), La Jolla, 2017.

Matsuoka, N., Murton, J.: Frost weathering: recent advances and future directions. Permafrost Periglac., 19, 195-210, https://doi.org/10.1002/ppp.620, 2008.

Meinzer, O. E.: The history and development of ground–water hydrology. J Washington Academy of Sciences, 24,

535   6-32, http://www.jstor.org/stable/24532897, 1934.

Mollo, L. and Greco, R.: Moisture measurements in masonry materials by time domain reflectometry. J. Mater. Civil Eng., 23, 441-444, 2011.

Nguyen, J. L., Schwartz, J. and Dockery, D. W.: The relationship between indoor and outdoor temperature, apparent temperature, relative humidity, and absolute humidity, Indoor Air, 24, 103–112,

540   https://doi.org/10.1111/ina.12052, 2013.

Rempe, D. M. and Dietrich, W. E.: Direct observations of rock moisture, a hidden component of the hydrologic cycle, P. Natl. Acad. Sci. USA, 115, 2664–2669, https://doi.org/10.1073/pnas.1800141115, 2018.

Sakaki, T. and Rajaram, H.: Performance of different types of time domain reflectometry probes for water content measurement in partially saturated rocks, Water Resour. Res., 42, W07404, https://doi.org/10.1029/2005WR004643, 2006.

Salve, R., Rempe, D. M. and Dietrich, W. E.: Rain, rock moisture dynamics, and the rapid response of perched

545   groundwater in weathered, fractured argillite underlying a steep hillslope, Water Resour. Res., 48, 1–25, https://doi.org/10.1029/2012WR012583, 2012.

Sass, O.: Rock moisture measurements: techniques, results, and implications for weathering. Earth Surf. Proc. Land, 30, 359–374, https://doi.org/10.1002/esp.1214, 2005.

Schmidt, L. and Rempe, D.: Quantifying dynamic water storage in unsaturated bedrock with borehole nuclear

550   magnetic resonance, Geophys. Res. Lett., 47, e2020GL089600, https://doi.org/10.1029/2020GL089600, 2020.

Schoups, G., Hopmans, J. W., Young, C. A.,Vrugt, J. A. and Wallender, W.W.: Multi-criteria optimization of a regional spatially-distributed subsurface water flow model, J. Hydrol., 31, 20–48, https://doi.org/10.1016/j.jhydrol.2005.01.001, 2005.

555   Shapley, L.S., 1953. A value for n-person games, in: Contributions to the Theory of Games II, editd by: Kuhn, H. and Tucker, A., Princeton University Press, Princeton, 307–317, https://doi.org/10.1515/9781400881970-018, 1953.

Štrumbelj, E. and Kononenko, I.: Explaining prediction models and individual predictions with feature contributions, Knowl. Inf. Syst. 41, 647–665, https://doi.org/10.1007/s10115-013-0679-x, 2014.

560   Sun, Z. H. and Scherer, G. W.: Measurement and simulation of dendritic growth of ice in cement paste, Cement Concrete Res., 40, 1393–1402, https://doi.org/10.1016/j.cemconres.2010.03.008, 2010.

Tindall, J., Kunkel, J. and Anderson, D. E.: Unsaturated Zone Hydrology for Scientists and Engineers, Pearson Education Inc., New York, 1998.

Vereecken, H., Huisman, J. A., Pachepsky, Y., Montzka, C., van der Kruk, J., Bogena, H., Weihermuller, L.,
565   Herbst, M., Martinez, G. and Vanderborght, J.: On the spatio-temporal dynamics of soil moisture at the field scale, J. Hydrol., 516, 76–96, https://doi.org/10.1016/j.jhydrol.2013.11.061, 2014.

Vinnikov, K. Y., Robock, A., Speranskaya, N. A., and Schlosser, C. A.: Scales of temporal and spatial variability of midlatitude soil moisture, J. Geophys. Res.-Atmos., 101, 7163–7174, https://doi.org/10.1029/95JD02753, 1996.

570   Wang. X. S., Wan, L., Peng, T., Dong, P. and Qian, J.: Infiltration water in Yungang Grottoes and its movement, Geotechnical Investigation & Surveying, 40, 12–16, 2012. (in Chinese)

Xiang, Z. R., Yan, J. and Demir I.: A rainfall-runoff model with LSTM-based sequence-to- sequence learning, Water Resour. Res., 56, e2019WR025326, https://doi.org/10.1029/2019WR025326, 2020.

Xie, H. Y., Jiang, X. W., Tan, S. C., Wan, L., Wang, X. S., Liang, S. H. and Zeng, Y. J.: Interaction of soil water
575   and groundwater during the freezing–thawing cycle: field observations and numerical modeling, Hydrol. Earth Syst. Sci, 25,4243–4257, https://doi.org/10.5194/hess-25-4243-2021, 2021.

Xu, L., Lio, A., Hu, J., Ogletree, A. D. F. and Salmeron, M.: Wetting and capillary phenomena of water on mica, J. Phys. Chem. B, https://doi.org/10.1021/JP972289L, 1998.

Yu, L. Y., Zeng, Y. J., Su, Z. B., Cai, H. J. and Zheng, Z.: The effect of different evapotranspiration methods on
580   portraying soil water dynamics and ET partitioning in a semi-arid environment in Northwest China. Hydrol. Earth Syst. Sci., 20, 975–990, https://doi.org/10.5194/hess-20-975-2016, 2016.

Yu, L., Zeng, Y., Wen, J. and Su, Z: Liquid-Vapor-Air Flow in the Frozen Soil. J. Geophys. Res.-Atmos., 123, 7393-7415, https://doi.org/10.1029/2018jd028502, 2018.

Zhang, Z. Y., Wang, W., Gong, C. C., Wang, Z. F., Duan, L., Yeh, T. J. and Yu, P. Y.: Evaporation from seasonally
585   frozen bare and vegetated ground at various groundwater table depths in the Ordos Basin, Northwest China. Hydrol. Process., 33, 1338-1348, https://doi.org/10.1002/hyp.13404, 2019.

Zhao, H. F., Li, J., Yuan, Q. Q., Lin, L. P., Yue, L. W. and Xu, H. Z.: Downscaling of soil moisture products using deep learning: Comparison and analysis on Tibetan Plateau, J. Hydrol., 607, 127570, https://doi.org/10.1016/j.jhydrol.2022.127570, 2022.

590   Zhao, Z., Chen, W. H., Wu, X. M., Chen, P. C. Y. and Liu, J. M.: LSTM Network: a deep learning approach for short-term traffic forecast, IET Intell. Transp. Sy., 11, 68–75, https://doi.org/10.1049/IET-ITS.2016.0208, 2017.

Zhu, Y., Irmak, S., Jhala, A. J., Vuran, M. C. and Diotto, A.: Time-domain and frequency-domain reflectometry type soil moisture sensor performance and soil temperature effects in fine- and coarse-textured soils, Appl.
595   Eng. Agric., 35, 117–134, https://doi.org/10.13031/aea.12908, 2019.